

# Interactive Segmentation of Vascular Structures in CT Images for Liver Surgery Planning

L. Wang<sup>1</sup>, C. Hansen<sup>1</sup>, S. Zidowitz<sup>1</sup>, H. K. Hahn<sup>1</sup>

<sup>1</sup> Fraunhofer MEVIS, Institute for Medical Image Computing, Bremen, Germany

Contact: lei.wang@mevis.fraunhofer.de

## Abstract:

Vasculature analysis based on CT images is indispensable in liver surgical planning and diagnosis of liver disease. We propose a novel framework and efficient workflow with minimal user interactions to analyze liver vasculature in multi-phase CT images. To ensure segmentation quality and efficiency, a set of semi-automatic algorithms are applied to initially segment different vascular structures in different phase. A fully automatic vessel separation procedure runs parallel to separately connected hepatic and portal veins. In addition, an interactive editing method is integrated into the framework to refine the segmentation of each individual structure. Quantitative evaluations of segmented vessels conducted for 60 test data sets are demonstrated.

Keywords: Liver surgery planning, vascular segmentation, computer-assisted surgery

## 1 Purpose

The segmentation of vascular structures in the liver is required to explore patient-individual branching patterns. Combined with tumor segmentation, spatial relations between vessels and tumors can be quantitatively analyzed. The segmentation of vessels builds the basis for vascular risk analyses [1] and virtual resection planning [2]. In addition, labeling vessels helps identify vascular territories. However, the complexity of vasculature and low contrast between vessels and surrounding tissues due to imperfect acquisition make these tasks challenging. In this work, we present a dedicated analysis framework of hepatic vein (HV), portal vein (PV), hepatic artery (HA), and bile duct (BD) for liver surgery planning in multi-phase computer tomography (CT) images.

## 2 Material and Method

The workflow consists of two primary steps:

- Vascular structure segmentation and separation
- Interactive segmentation editing

The processing pipelines for different selected phases also vary. Figure 1 illustrates the processing pipelines for HV/PV, HA, and BD phases.

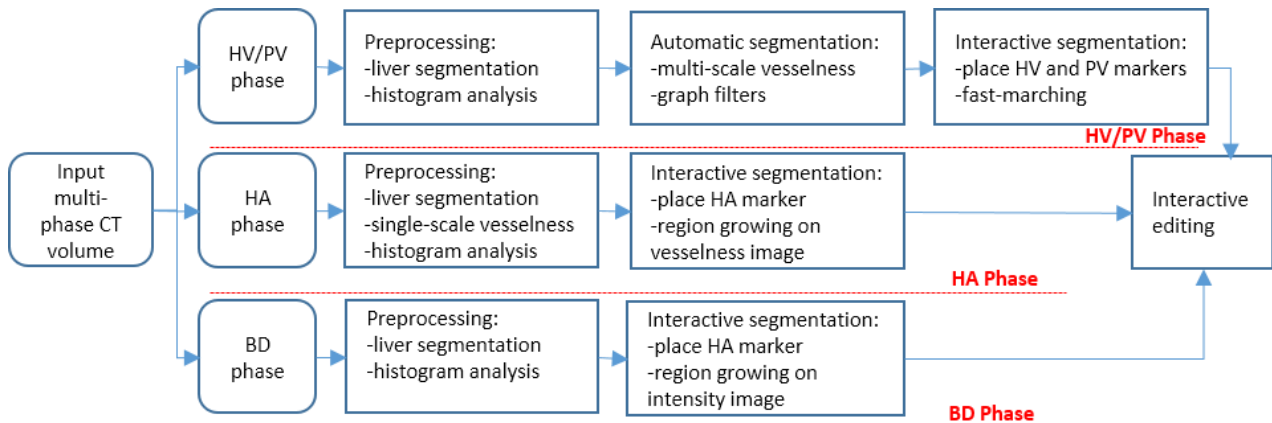


Fig. 1 Schematic overview of the entire processing workflow for HV/PV, HA, and BD phases

## 2.1 Vascular structure segmentation and separation

### *HV/PV segmentation*

Adequate delineation of HV and PV is important for liver surgical planning. During acquisition of multi-phase CT images, both of these venous vessels are enhanced and acquired either in a common phase or in two individual phases. The presence of large lesions and inadequate enhancement of venous vessels, which especially occur during imperfect image acquisition in oncological patients, make the segmentation task quite challenging. To overcome these difficulties, we employ a semi-automatic segmentation framework requiring minimal user interactions for quick and robust segmentation of hepatic vein and portal vein presented in common or individual phases. First, in the preprocessing stage, we segment the liver on the selected venous phase and analyze the histogram of intensities to preclude regions with extremely low intensities.

Hessian-based filters have been widely employed to enhance tube-like structures of 3D images. There are plenty of vesselness filters published in previous works [3] [4]. Because the contrast level of venous vessels in different input images are quite heterogeneous, we choose the multi-scale, Hessian-based vesselness filter introduced by Frangi et al. to enhance vessels of CT volume within the liver mask [3]. Major benefits of Frangi's vesselness filter include incorporation of information from all three Eigen values and independence from their absolute values, which are associated with absolute contrast level of vessels; its output is scaled in range of 0 and 1. Assuming the eigenvalues of Hessian matrix are sorted in order:  $|\lambda_1| \leq |\lambda_2| \leq |\lambda_3|$ , the Frangi's vesselness filter is defined as following:

$$f(\sigma) = \begin{cases} \mathbf{0} & \text{if } \lambda_2 > \mathbf{0} \text{ or } \lambda_3 > \mathbf{0} \\ \left(1 - \exp\left(-\frac{R_A^2}{2\alpha^2}\right)\right) * \exp\left(-\frac{R_B^2}{2\beta^2}\right) * \left(1 - \exp\left(-\frac{S^2}{2c^2}\right)\right) & \end{cases}$$

where  $R_A = \frac{|\lambda_2|}{|\lambda_3|}$ ,  $R_B = \frac{|\lambda_1|}{\sqrt{|\lambda_2\lambda_3|}}$  and  $S = \sqrt{\lambda_1^2 + \lambda_2^2 + \lambda_3^2}$ . The ratio  $R_A$  is designed to differentiate vessels from sheet-like structures, whereas  $R_B$  is used to distinguish vessels from blob-like structures. The term  $S$  aims to suppress noise structures. The scale parameter  $\sigma$  indicates the size of Gaussian kernel used for calculating Hessian matrix. The parameters used in this filter,  $\alpha, \beta, c$  are set to 0.5, 0.5, and 10. Considering the radius range of HV and PV, we choose three optimized scales for  $\sigma$ : 1.5 mm, 2.25 mm, and 3 mm based on our experimental tests, which are able to capture vessels with thin, medium, and thick radii (see Fig. 2(a)). The ultimate vesselness response is obtained by extracting the maximum across all scales. Normally, calculating the Hessian matrix is quite expensive when increasing the Gaussian kernel size. To speed up the vesselness filter, we adopt an inverse multi-scale strategy which keeps the kernel size constant at 1.5mm, but downsamples input volumes to larger voxel spacing.

On the basis of vesselness response, we initially segment the HV and PV utilizing an automatic region-growing algorithm. Through histogram analysis, all voxels with a vesselness value between 90<sup>th</sup> and 99<sup>th</sup> percentiles are taken as seed points. The lower and upper thresholds of region growing are chosen as 75<sup>th</sup> percentile and maximal response, respectively. If the HV and PV possess high contrast against their surroundings, initial segmentation normally yields satisfactory results (see Fig. 2(b)). Nevertheless, for the cases where HV and PV exhibit extremely low contrast or where large hypodense lesion areas with internal hyperdense structures are present, many irrelevant structures will be enhanced by the vesselness filter and captured in region-growing step. Therefore, we first transform the segmented vessel tree structure into a graph representation [5] and validate the graph tree using two criteria:

- 1) The volume of each independent graph tree should exceed a lower limit  $T_{min}$ .
- 2) The edge length of branches should be longer than a minimum threshold  $E_{min}$ .

These two graph filters can rule out most irrelevant tree structures and prune disturbing branches. Other issues lie in the areas of inferior vena cava and entrance of PV, which are normally not enclosed by the segmented liver mask. Moreover, the inferior vena cava can be hypodense or hyperdense depending on the contrast agent density. We propose a robust interactive solution to recover the segmentation in both regions. Two markers need to be placed in the regions where main branches of HV and PV are joined (see Fig. 2(c)). Then, a fast marching algorithm is applied in the predefined neighborhoods of these two markers [6]. The efficient computation of the algorithm permits instant display of segmented regions when marker positions are adjusted until optimal positions are reached.

### *HV/PV separation*

The HV and PV will be simultaneously segmented when they present in a common phase. For liver surgical planning, it is demanding to separate and analyze them individually. The separation process is triggered when HV and PV markers are placed. To meet computation time constraints, we employ an interactive watershed transform algorithm that takes the placed HV and PV markers as seed points of two different classes [7]. The cost images of watershed transforms are original intensity images smoothed with a diffusion filter. The entire volume will be classified into two classes associated

with HV and PV markers, respectively. Consequently, the segmented HV and PV can be separated into two classes when we overlay the class labels to segmentation result (see Fig. 2(d)).

#### *HA and BD segmentation*

Compared to HV and PV, segmentations of HA or BD are relatively less challenging because HA and BD normally show very high contrast against other structures in HA and BD phases. However, one issue that we observed in some of HA phases is that other vascular structures like HV and PV are slightly enhanced, and contrast enhancement of HA is heterogeneous. Hence, we use a single-scale vesselness filter again to enhance HA in the preprocessing step. The scale parameter of the kernel size is set to 1.0 mm. Afterwards, a semi-automatic region-growing scheme is conducted which requests a single marker placed in the HA or BD volume. The cost images used in region growing are vesselness response image and intensity image for HA and BD, respectively.

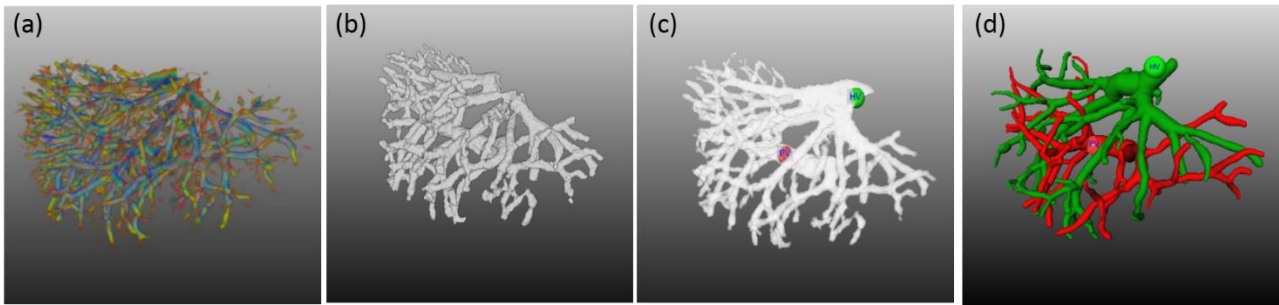


**Fig. 2** Illustration of HV/PV segmentation: (a) response of multi-scale vesselness filter represented with color map: red, green and blue indicates response of small, medium and large scales, respectively; (b) initial segmentation of HV and PV; (c) interactive refinement of HV and PV segmentation: HV and PV markers displayed with green and red dots; (d) result of separating HV and PV.

## 2.2 Interactive segmentation editing

To allow modification of the initial segmentation and separation results by the user, we provide a set of interactive editing methods. The methods are based on a graph structure (consisting of a set of edges and nodes) calculated from the existing segmentation mask. As an input for each editing step, only a single click point by the user is required. The following correction modes are available:

- Adding branches
- Deleting branches
- Relabeling branches (required for incorrect vessel separation)

Adding of branches is mainly based on a Dijkstra's algorithm, which uses the underlying CT image as a cost image. Giving a selected click point, the algorithm calculates the cheapest path from this point to the segmentation mask. This path builds the centerline for the new branch. Subsequently, vessel radii along the path are approximated using a ray casting algorithm that evaluates grey values around the centerline. Finally, the new branch is added to the existing graph structure.

While adding of branches is only applicable in 2D slices, the other two editing modes can also be applied by interacting with the 3D vessel models in the 3D viewer. Analogous to the adding mode, only a single click point by the user is required. For deleting and re-labeling of branches, the user controls the influence of the correction by selecting either a local or a global influence. For the local influence mode, only the edge that is selected by the user is modified. For the global influence mode, all parent edges are modified, i.e. removed or re-labeled. With these three correction modes, the user is provided with necessary tools to refine the results of vascular segmentation and separation steps describe in section 2.1.

## 3 Results

To evaluate the performance of presented segmentation techniques, a test data set enclosing 60 multi-phase hepatic CT scans acquired from 30 liver donors and 30 oncological patients was collected. HV/PV phases were taken for all scans. Depending on diagnostic circumstances, HA and BD phases were not always present in original scans. Segmenting HA and BD is relatively less challenging compared to HV/PV segmentation, and the results were normally satisfactory after a few manual correction steps. Therefore, in this work, we quantitatively evaluated the quality of HV/PV segmentation. The vasculatures of HV/PV were manually segmented by experienced radiologists which were used as reference for quantitative evaluation. In addition, the markers used to refine the segmentation in areas of inferior vena cava and entrance

of PV were placed manually and saved prior to automatic testing. The image resolution of HV/PV phases in test images could range from  $512 \times 512 \times 189$  to  $512 \times 512 \times 310$ . The calculation of multi-scale vesselness filter takes 15 to 40 seconds depending on the amount of vasculatures presented in the scans. The initial segmentation and subsequent refinement of HV/PV take maximally 3 seconds using a 3.07 GHz Intel CPU.

The Dice Coefficient (DC) is computed to measure the overlap between segmented HV/PV and the ground truth. It is able to reflect both misalignment of branches and errors of radii. Additionally, we introduce another metric to further review the alignment between segmented and reference vessel trees. The percentage of the skeleton of segmented vessels covered by the reference vessel mask is calculated, and the same percentage is computed inversely for the skeleton of reference vessels. The average of two percentages depicts the branching consistency of both vessel trees. Table 1 listed the statistical results of DC and branching alignment (BA) for all test cases. It is easy to observe that the branching alignment BA1 is larger than BA2 on average. The reason is that the reference vessel tree tends to delineate the complete vessel structures including very thin vasculatures whose radii are less than 1mm, which are of less interest for liver surgical planning.

	DC	BA1 (Seg to Ref)	BA2 (Ref to Seg)	BA
Mean	0.51	0.78	0.51	0.64
Standard deviation	0.11	0.19	0.13	0.11

**Table 1.** Statistics of quantitate evaluations: BA1 and BA2 indicates the branching alignment from segmentation (Seg) to reference (Ref) and vice versa. BA shows the average of BA1 and BA2

## 4 Discussion

Multi-scale vesselness filter is sensitive in detecting vascular structures in different contrast levels. Increasing the number of scales will deliver better enhancement response for the vessels with various radii. Considering the balance between performance and computational expense, we choose three scales in this work, which consumes the time in acceptable range. Further experiments are required to investigate how performance relates to the scale numbers. In practice, the disturbing structures resembling vasculatures locally will be enhanced as well, especially in the patients with oncological lesions. The graph filters and manual editing tool in post-processing step are capable of ruling out these false positives. The optimal parameter settings for the graph filters used in post-processing were obtained through a brutal test iterating through all possible combinations. The success of Water-Shed transform algorithm used in separation of HV and PV depends on the marker positions. We search for the local maxima in the near of two placed seed markers and extend number of seeds by adding neighboring points. The correction of seed markers helps to improving the robustness and reliability of the separation method. Generally, segmenting HA and BD using region-growing based methods yields reasonably good results due to the high contrast. Unsatisfactory segmentation can be efficiently corrected manually in editing step. Due to the time constraints, we did not adopt advanced segmentation techniques such as level-set or graph-based methods, which could be parts of our future works.

## 5 References

- [1] C. Hansen, S. Zidowitz, M. Hindennach, A. Schenk, H. Hahn, and H. O. Peitgen, *Interactive determination of robust safety margins for oncologic liver surgery*, Int J Comput Assist Radiol Surg, vol. 4, no. 5, pp. 469–474, 2009.
- [2] O. Konrad-verse, B. Preim, and A. Littmann, *Virtual Resection with a Deformable Cutting Plane*, SimVis, no. 1, 2004.
- [3] A. F. Frangi, W. J. Niessen, K. L. Vincken, and M. A. Viergever, *Multiscale vessel enhancement filtering*, in MICCAI, vol. 1496, pp. 130–137, 1998.
- [4] M. Descoteaux, D. L. Collins, and K. Siddiqi, *A geometric flow for segmenting vasculature in proton-density weighted MRI*, Medical image analysis, vol. 12, no. 4, pp. 497–513, Aug. 2008.
- [5] D. Selle, B. Preim, A. Schenk, and H.-O. Peitgen, *Analysis of vasculature for liver surgical planning*, IEEE transactions on medical imaging, vol. 21, no. 11, pp. 1344–57, Nov. 2002.
- [6] J. A. Sethian, *A fast marching level set method for monotonically advancing fronts*, Proceedings of the National Academy of Sciences, vol. 93, no. 4, pp. 1591–1595, 1996.
- [7] H. Hahn and H. Peitgen, *The skull stripping problem in MRI solved by a single 3D watershed transform*, MICCAI, pp. 134–143, 2000.